Mechanical Characteristics and Metallurgical Properties of GTAW-SMAW Hybrid Welding on TMCP Steel Grade EH36 Butt Weld Parts

Sumeth Nuchim
Department of Mechanical Engineering, Faculty of Engineering, Srinakharinwirot University, Ongkharak, Nakhonnayok, Thailand
sumeth.nuchim@g.swu.ac.th

Phacha Bunyawanichakul
Department of Mechanical Engineering, Faculty of Engineering, Srinakharinwirot University, Ongkharak, Nakhonnayok, Thailand
prachabu@g.swu.ac.th

Tri Kharanan
Department of Mechanical Engineering, Faculty of Engineering, Srinakharinwirot University, Ongkharak, Nakhonnayok, Thailand
tri.kharanan@g.swu.ac.th

Teerapath Limboonruang
Department of Mechanical Engineering, Faculty of Engineering, Srinakharinwirot University, Ongkharak, Nakhonnayok, Thailand
teeerapath@g.swu.ac.th

Nittalin Phunapai
Department of Mechanical Engineering, Faculty of Engineering, Srinakharinwirot University, Ongkharak, Nakhonnayok, Thailand
nittalin@g.swu.ac.th

Natchanun Angsuseranee
Department of Manufacturing Engineering, Faculty of Engineering and Architecture, Rajamangala University of Technology Suvarnabhumi, Phra Nakhon Si Ayutthaya (Huntra), Thailand
natchanun.a@rmutsb.ac.th (corresponding author)

Visanu Boonmag
Department of Mechanical Engineering, Faculty of Engineering, Thonburi University, Bangkok, Thailand
visanu@thonburi-u.ac.th

Sasikan Suwanprateep
Department of Industrial Engineering, Rajamangala University of Technology Suvarnabhumi, Thailand
sasikan.s@rmutsb.ac.th

Sukit Litikorn
Engineering Support Division at Harn Engineering Solutions Public Company Limited, Thailand
sukit@yahoo.co.th

Received: 15 November 2025 | Revised: 4 January 2026 and 23 January 2026 | Accepted: 2 February 2026

 DOI: https://doi.org/10.48084/etasr.16287

ABSTRACT

The successful application of the Thermo-Mechanical Control Process (TMCP) in combination with the latest innovative technologies has stimulated the development of EH36 steel plates. This type of steel is often welded by Shielded Metal Arc Welding (SMAW), but there is no hybrid welding of steel sheets. The main objective of this study is to investigate the mechanical characteristics and metallurgical properties of TMCP grade EH36 steel plates of Gas Tungsten Arc Welding (GTAW) and SMAW hybrid welding processes. The steel plate used in the study measured 650 × 170 mm and had a thickness of 12 mm. Mechanical characteristics and metallurgical tests revealed deep penetration and melting between filler metal and base metal, indicating perfection between the weld metal and base metal. The hybrid GTAW and SMAW welding process produced an average maximum tensile strength of 524.35 MPa. The maximum hardness in the weld metal zone was 231 HV, and the lowest hardness in the base metal was 168 HV. The impact test results showed that the energy absorbed in the Heat-Affected Zone (HAZ) was 256.57 J, which was higher than the energy absorbed in the weld metal zone (184.34 J), indicating that the HAZ had better toughness than the weld metal zone. The microstructure of the weld metal mainly comprised acicular ferrite phase, which resulted in the weld metal being harder than the base metal.

Keywords-GTAW-SMAW hybrid welding; EH36 steel plates; mechanical characteristics; metallurgical

I. INTRODUCTION

Thick steel plates are widely used in the shipbuilding industry. The demand for heavy thick plates is due to their high strength, toughness, and weldability properties, making them popular for use in the construction of large container ships. The successful application of the TMCP combined with innovative technologies has fueled the development of EH36, EH40, and EH47 grades. These grades include metals, such as boron, copper, and nickel, in addition to tightly controlled rolling and cooling processes to simultaneously improve strength and toughness. EH36 high-temperature welding steel plates were developed to exhibit good toughness at the melting point by enhancing the thermal stability of TIN particles at high temperatures. These thick steel plates are commonly utilized in structural parts of the shipbuilding, oil, and gas industries [1].

Welding is employed in engineering because it provides significant advantages, such as greater design flexibility, reduced manufacturing costs, and weight savings, compared to other joining methods. Numerous welding techniques have been developed, and their advancement remains a key area of interest for many industrial sectors [2]. GTAW is a widely adopted technique that is particularly suitable for precision welding of thin metal sheets. Its high level of process control and relatively low equipment cost make it ideal for a broad range of materials [3]. SMAW is a welding process deployed for EH36, due to its simplicity, low cost, and portability [4]. The welding method for TMCP grade EH36 for hull shell plates in the shipbuilding industry has changed from the previous welding process of SMAW for all pass line welding to hybrid welding, GTAW, and SMAW. Both welding processes are used to complete the joint, with the root pass performed using the GTAW process while subsequent passes are completed using the SMAW process. This combination leverages the respective quality advantages of each method [5].

The mechanical and metallurgical characteristics of welds have been investigated. Authors in [6] examined the effects of hybrid GTAW-SMAW welding parameters on the hardness of the weld metal and the HAZ in low-carbon steel. Their research focused on factors such as gas flow rate and inter-pass temperature differences between the GTAW and SMAW processes. It was found that weld hardness was primarily influenced by the GTAW current, while the SMAW current had a more significant effect on the HAZ hardness. Authors in [7] studied the influence of the welding procedure and Post-Weld Heat Treatment (PWHT) on HSLA steels. The findings showed that the mechanical properties of high-strength steels welded using the Gas Metal Arc Welding (GMAW) process were comparable to those obtained through the SMAW process. Moreover, PWHT can be applied without causing significant changes to the mechanical properties. The GMAW process also offers increased productivity while maintaining high strength and good quality in welded steel. Authors in [8] conducted an experiment in which carbon steel filler metal was added to the base metal of stainless-steel clad sheets. It was revealed that the weld zone contained alloying elements from both stainless steel and carbon steel, leading to the formation of a martensitic phase in the first weld layer due to the use of the carbon steel filler. Moreover, a phase transformation resulted in greater hardness in the weld metal than in the base metal. Additionally, cracks were observed to initiate near the HAZ of the specimen.

Authors in [9] investigated the mechanical properties of dissimilar butt joints between Ni medium-manganese (M-Mn) and nickel-chromium (Ni-Cr) austenitic stainless steels processed using GTAW. The resulting microstructure in the weld zone consisted of an austenitic matrix with delta ferrite. Despite successful joining, the weld exhibited a relatively low tensile strength of 610 MPa, which is significantly lower than that of both base metals (M-Mn SS and Ni-Cr SS). This reduction in strength was attributed to the presence of an uneven dendritic structure in the weld zone, along with chromium carbide (Cr-carbide) precipitation. Authors in [10] compared the microstructure and mechanical properties of high-strength and tough ship steel plates. It was demonstrated that the microstructure of E36, EH36, and FH36 ship plate steel consisted of polygonal ferrite, pearlite, and granular carbides. In particular, EH36 and FH36 ship steel plates had higher

strength than E36 ship steel plates. Authors in [11] studied the microstructure affected by the heat input of hot-rolled ferritic steel XPF800. It was found that the optimum parameter for the current was 140 A, the welding speed was 100 mm/min, and the heat input was 0.62 kJ/mm in the GTAW of XPF800 plates.

Authors in [12] conducted butt welding of 30 mm thick EH36 shipbuilding steel plates using a two-pass technique that combined Hybrid Laser Arc Welding (HLAW) and Submerged Arc Welding (SAW). The results demonstrated high process stability, enabling defect-free welding of plasma-cut edges while achieving adequate mechanical and technological properties. Authors in [13] investigated austenitic stainless steels Inconel 718 and 304L using a combination of GTAW and SMAW, employing Ni-based filler materials ERNiCr-3 and ENiCrFe-3. A fully austenitic weld microstructure was found, containing Nb- and Ti-rich carbides within the interdendritic regions. Tensile testing at 600 °C indicated failure in the SS304L base metal, while the weld metal exhibited an impact toughness of 109 J lower than that of the base metal, which was likely due to NbC phase formation in the interdendritic zones. Authors in [14] investigated novel high-Mn austenitic steel welded joints, produced using SMAW, SAW, and GTAW for cryogenic applications in LNG tanks. The weld metals exhibited good welding quality, with weld hardness values below 280 HV, attributed to their fully austenitic microstructure. Authors in [15] carried out degradation tests to evaluate the changes in hardness and tensile strength of Shore A butt-welded PE100 SDR11 pipes used in natural gas distribution. Alterations in the tensile strength of the welded joints increased with longer curing times by 6.5% after 10 years and 6.16% after 20 years. In contrast, unwelded samples experienced a 3.57% decrease in tensile strength after 10 years but showed a 5.84% increase after 20 years. The Shore A hardness remained largely unaffected by artificial aging over both 10-year and 20-year periods.

Despite the extensive research on metal welding across various fields, the application of hybrid welding processes in industry remains limited. Therefore, this study investigates the effects of a hybrid welding approach on the mechanical and microstructural characteristics of butt joints in EH36 steel plates. The welding procedure begins with GTAW for the first pass, followed by SMAW for the second to fourth passes. The study focuses on analyzing the weld metal and the HAZ through Energy Dispersive Spectroscopy (EDS) and microstructural examination of impact fracture in the specimen. In addition, the mechanical properties of the welded joints are evaluated. Finally, the experimental results are analyzed and summarized to assess the effectiveness of the hybrid welding process.

II. MATERIALS AND METHODS

A. Welding Procedure

The GTAW and SMAW hybrid welding processes of TMCP were conducted on EH36 steel plates. The chemical composition of the base metal is detailed in Table I [16]. For GTAW, filler metal A5.18 ER 70S-6 was utilized, with its chemical makeup presented in Table II [17].

TABLE I. CHEMICAL COMPOSITION OF EH36 STEELS [16]

Grade	EH36
C	0.144
Si	0.326
Mn	1.40
P	0.0152
S	0.0067
Nb	0.027
V	0.024
Mo	0.006
Cr	< 0.005
Cu	0.01
Ti	0.011
Ni	0.006
Al	0.047

TABLE II. CHEMICAL COMPOSITION OF AWS A5.18 ER 70S-6 [17]

Filler metal (GTAW)	AWS A5.18 ER 70S-6
C	0.04
Si	0.85
Mn	1.46
P	0.012
S	0.014
Cu	0.11
Cr	0.02
Ni	0.01
Mo	0.01
V	0.01

In the case of SMAW, filler metal AWS A5.1 E7016 was employed, and its chemical composition is provided in Table III [18] The dimensions and welding process of two steel plates using a V-groove angle of 60° is shown in Figure 1. The hybrid welding parameters of GTAW and SMAW are listed in Tables IV and V [16], respectively. Figure 2 illustrates the welding process performed on the root pass using GTAW and SMAW. Figure 3 depicts the welding process applied to a capping pass weld in the 1G welding position, in accordance with the AWS D1.1 standard.

The heat input was calculated using [13]:

$$HI = \frac{V \times I \times 60}{S} \quad (1)$$

where HI is the heat input (kJ/mm), V is the arc voltage (V), I is the welding current (A), and S is the travel speed (mm/s).

A total of four weld passes were employed to fill the groove. The backing pass was executed using the GTAW process. The welding parameters for the root pass, filling passes, and backing passes are provided in Table VI.

B. Mechanical Property Test

For the mechanical test, experiments were conducted for four methods. The first step was the tensile test using the tensile machine model INSTROL: UTM 2000 kN, as shown in Figure 4. This machine was utilized to test the longitudinal tensile force of all weld metals by preparing the test piece to be reduced in size. The experiment can input the parameter value directly from the monitor. The test processing was in the form of numbers and graphs. In this research, the tensile test was used to find the ultimate tensile strength of the weld as well as

the yield strength and the percentage of elongation [11]. The parameter values of the tensile test specimen were set according to the ASTM E8M-22 standard, as illustrated in Figure 5.

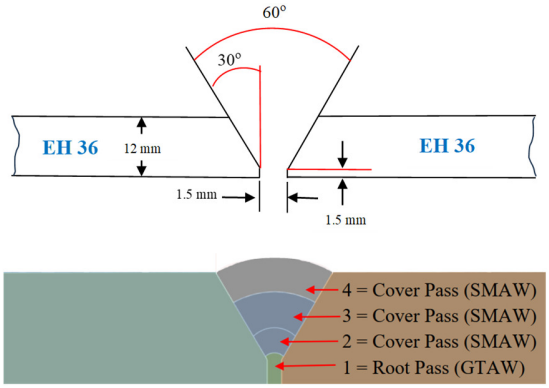

Fig. 1. Dimensions of two steel plates and hybrid welding procedure.

Fig. 2. GTAW-SMAW hybrid welding process on the root pass.

Fig. 3. GTAW-SMAW hybrid welding process on the capping pass.

TABLE III. CHEMICAL COMPOSITION OF AWS A5.1 E7016 [18]

Filler metal (SMAW)	AWS A5.1 E7016
C	0.08
Si	0.64
Mn	0.86
P	0.012
S	0.008

TABLE IV. WELDING PARAMETER FOR GTAW [16]

Parameter	GTAW
Electrode type	AWS A5.18 ER 70S-6
Electrode diameter	2.4 mm
Current intensity	120 A
Welding speed	59.1667 mm/min
Shielding gas flow volume	16 liters/min

TABLE V. WELDING PARAMETER FOR SMAW [16]

Parameter	SMAW
Electrode type	AWS A5.1 E7016
Electrode diameter	3.2 mm
Current intensity	120 A
Welding speed-cover pass 2	46.43 mm/min
Welding speed-cover pass 3	32.50 mm/min
Welding speed-cover pass 4	38.23 mm/min

TABLE VI. PARAMETER FOR GTAW-SMAW HYBRID PROCESS

Welding passes	Welding process	Welding current (A)	Welding voltage (V)	Welding speed (mm/s)	Heat input for each pass (kJ/mm)
Root pass 1	GTAW	~120	~12	0.986	0.0876
Cover pass 2	SMAW	~120	~25	0.774	0.232
Cover pass 3	SMAW	~120	~25	0.542	0.332
Cover pass 4	SMAW	~120	~25	0.637	0.282

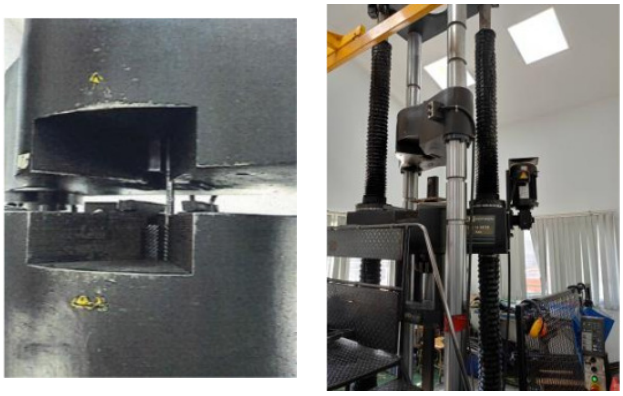

Fig. 4. Tensile testing machine INSTROL: UTM 2000 kN.

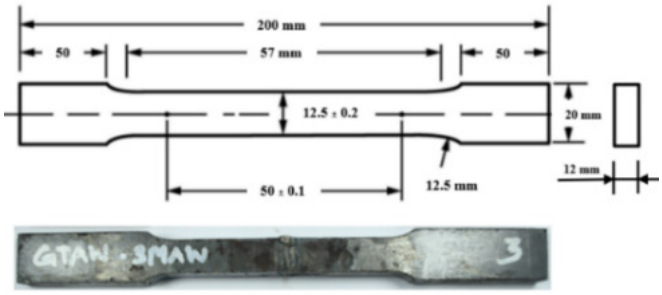

Fig. 5. ASTM E8M-22 standard tensile test specimen.

The second step involved bending tests, three types of which were conducted based on the direction of the applied

compressive forces. The specimens, prepared in accordance with ASTM E190-21, as illustrated in Figure 6, were tested on welds produced deploying the hybrid-welding process using GTAW and SMAW. Six specimens were pre-ground to remove excess weld metal before testing. The bending tests included side bend, face bend, and root bend [8].

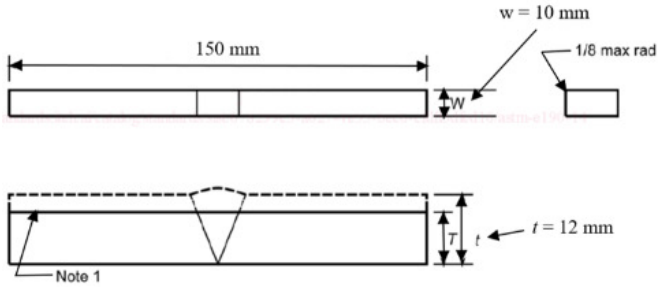

Fig. 6. ASTM E190-21 standard bending test specimen.

The third step was the Charpy impact test, which involved striking the test piece once with a swing to break it under specified conditions [13]. The specimen was required to be V-notch with the size and characteristics specified in ASTM E23-24. A total of three pieces per test point of the weld were obtained from the weld metal zone and HAZ, as displayed in Figure 7.

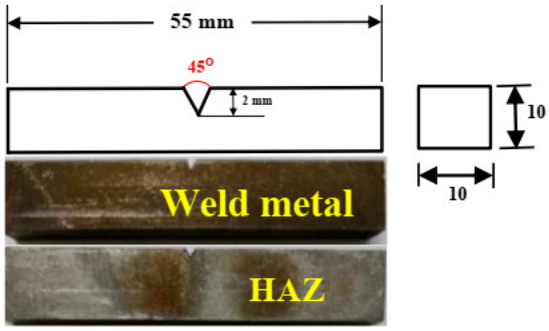

Fig. 7. ASTM E23-24 standard impact test specimen.

The fourth step was the hardness test, which was performed using a Vickers hardness tester model SHIMADZU: HMV-G. The test was performed according to the ASTM E3-11 standard using a force of 200 kgf and a holding time of 15 s [13, 14]. Compression was initiated on 3 lines: the bottom line of the GTAW welding pass, the middle line, and the top line of the SMAW welding pass, with a total of 14 test points, as portrayed in Figure 8.

C. Metallurgical and EDS Techniques

The metallographic structure examination was performed using a 3D laser microscope model LEXT OLS4100, which captured the details of the workpiece in 3D at high resolution. The experiment examined the microstructure at five points, as shown in Figure 9, to investigate the grain structure and the phase change melting behavior after the welding process. The five points examined were: the base metal of EH36 (base metal); the weld metal zone using the SMAW method (weld metal 1); the HAZ using SMAW metal (HAZ 1 SMAW); the weld metal using the GTAW method (weld metal 2); and the HAZ using the GTAW method (HAZ 2 GTAW). In addition, alloy composition was examined using the EDS technique with a JEOL JSM-7800F Prime (SEM) to analyze the chemical composition of specific elements in the weld metal, and thus prove which elements increased after the welding process was complete [9, 10].

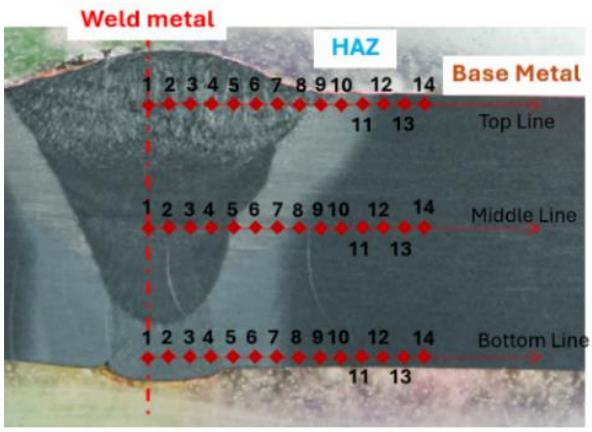

Fig. 8. Location of the hardness test: 3 lines, with 14 points in each line.

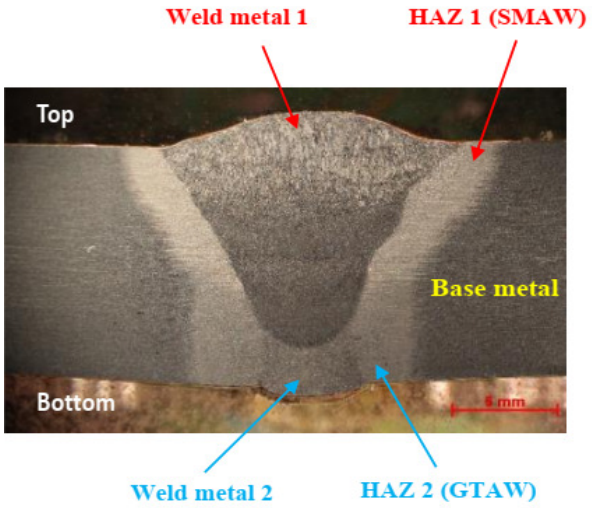

Fig. 9. Location of 5 points used for metallurgical structure inspection.

III. RESULTS AND DISCUSSION

A. Tensile Test Properties

Tensile tests were performed in the laboratory at 24.3 °C with 45% relative humidity. The former were conducted on a total of four specimens prepared using hybrid welding, GTAW, and SMAW processes. The tensile test results are presented in Table VII, and the plot of the stress-strain relationship between the welded between stress–strain is shown in Figure 10. The results indicate that the stress values were comparable across all specimens, as failure occurred through fracture in each case [22]. The average yield strength was 407.30 MPa, the average

ultimate tensile strength was 524.35 MPa, and the average percent elongation was 14.80%.

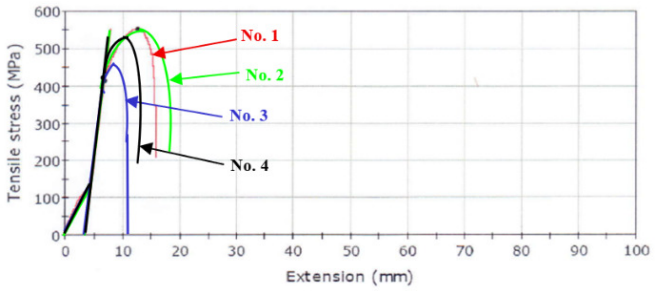

Fig. 10. Stress-strain curves of 4 specimens on hybrid welding by GTAW and SMAW.

However, it was also found that all fractures occurred in the HAZ, as illustrated in Figure 11. Therefore, the most fragile part of the specimen is the HAZ due to slow cooling during solidification. An increase in heat transmission during welding results in a larger grain size, which in turn decreases the material's toughness and reduces the difference between its yield strength and ultimate tensile strength. This is a critical phenomenon, particularly in the HAZ of a weld, where the base metal undergoes significant microstructural changes without melting.

Table VII presents the tensile test results. According to the shipbuilding standards for welding procedure qualification, the primary requirement is that the UTS of the weld must exceed the specified minimum standard for the base metal. Based on this criterion, all welds are considered acceptable if their UTS values surpass the standard threshold of 490 MPa [20]. However, the measured average UTS values are approximately 15.56% lower than the higher limits of the standard range for EH36 steel [20].

(a)

(b)

Fig. 11. Test specimen: (a) specimen before tensile test, (b) fractured specimen after tensile test.

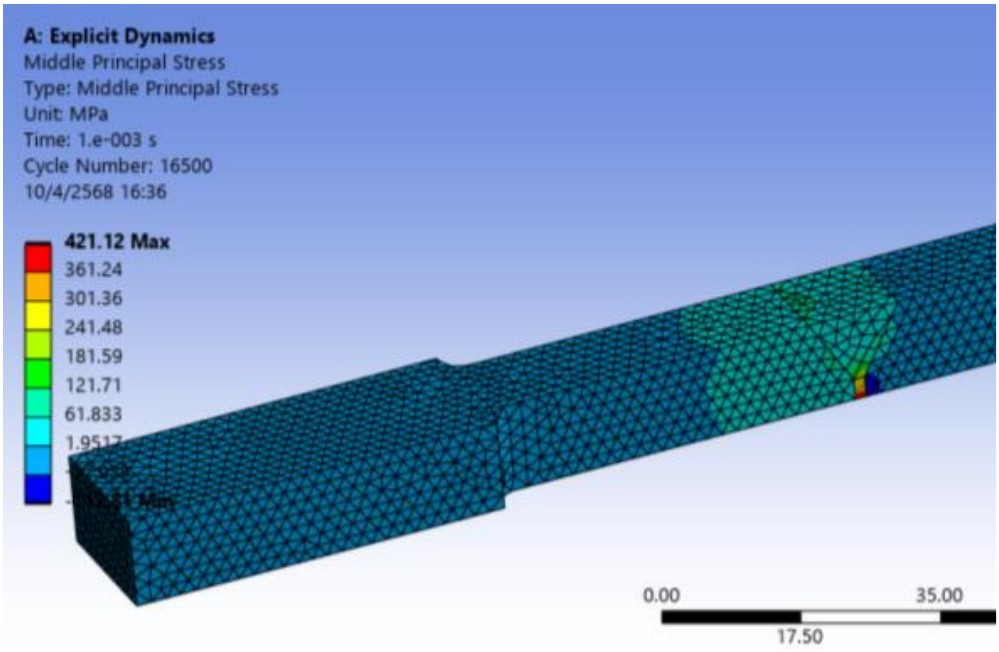

Fig. 12. Distribution of middle principal stress, showing a maximum value of 421.12 MPa.

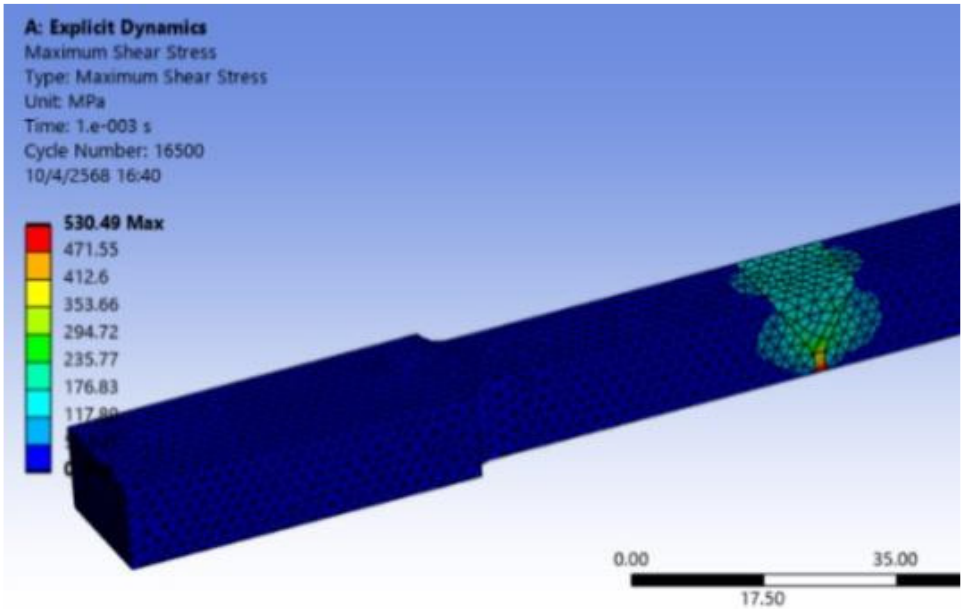

Fig. 13. Fig. 12. Distribution of maximum shear stress with a maximum value of 530.49 MPa.

TABLE VII. WELDED TENSILE TEST RESULTS

No.	Yield strength (MPa)	UTS (MPa)	Elongation %	Location of fracture
1	414.65	554.03	15.30	HAZ
2	405.32	554.64	19.50	HAZ
3	387.06	458.60	11.20	HAZ
4	422.17	530.13	13.20	HAZ
Average	407.30	524.35	14.80	HAZ
EH36 [20]	352.00	490-621	20	-

Tensile analysis was conducted using the numerical simulation from specimens with the same size and dimensions as the specimens tested in accordance with ASTM E8/E8M – 22, in which the triangular elements and a mesh size of 2 mm were chosen to perform the numerical simulation in the explicit dynamic mode, as shown in Figure 12. The obtained middle maximum principal stress was 421.12 MPa, compared to the experimental average yield strength of 407.30 MPa. The difference in the results of the two types of experiments was 3.39 % [21]. Figure 13 exhibits the maximum shear stress of 530.49 MPa, compared to the experimental UTS value of 524.35 MPa, with a difference of 1.17% [21].

Numerical simulations were employed only for comparison and final validation against experimental tensile test results to observe potential differences. This method helps researchers working with other steels estimate tensile stresses through simulation before experimental testing.

B. Bending Test Properties

Bending tests were conducted on hybrid-welded GTAW and SMAW specimens in accordance with ASTM E190:21, and under controlled conditions of 25 °C and 50% relative humidity. The specimens were subjected to a bend angle of 180° [8].

Table VIII summarizes the results of the three types of tests, while Figure 14 presents the corresponding macrostructures of six specimens after testing. In the lateral bending test, as depicted in Figure 14(a), only surface bulging was observed, with no visible cracks or fractures. The face bending test results are presented in Figure 14(b), and the root bending test results are displayed in Figure 14(c). All filled joints were found to be free from any cracks, fractures, tears, or other defects following the bending tests. Despite differences in the bending test types conducted on the filled joints and EH36 steel base material, the results indicated the absence of discontinuities, confirmingt that the welding processes used in fabricating the specimens were of high quality and reliability [8].

TABLE VIII. BENDING TEST RESULTS FOR GTAW AND SMAW HYBRID WELDED SPECIMEN

Type of bend	Mandrel diameter (mm)	Bend angle (degree)	Visual examination for surface discontinuity
Side bend	40	180o	No surface discontinuity
	40	180o	No surface discontinuity
Face bend	40	180o	No surface discontinuity
	40	180o	No surface discontinuity
Root bend	40	180o	No surface discontinuity
	40	180o	No surface discontinuity

C. Charpy Impact Test

The ASTM E23: 24 standard outlines the Charpy V-notch impact test, a method used to measure a material's toughness through its ability to withstand a sudden, forceful blow without fracturing. The impact test results are presented in Figure 15, which shows the fracture characteristics of the specimens at the weld metal before and after the impact test.

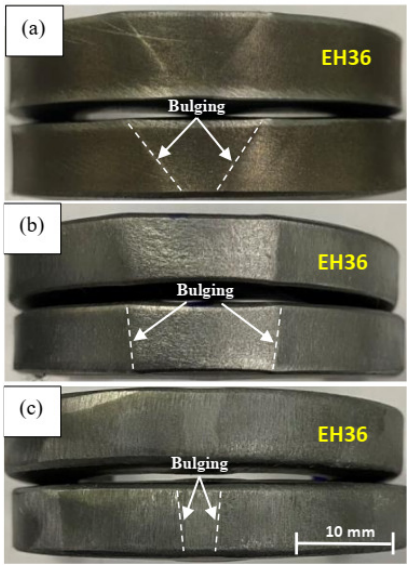

Fig. 14. Macrostructures of 6 specimens: (a) bulging after test side bend, (b) bulging after test face bend, and (c) bulging after test root bend.

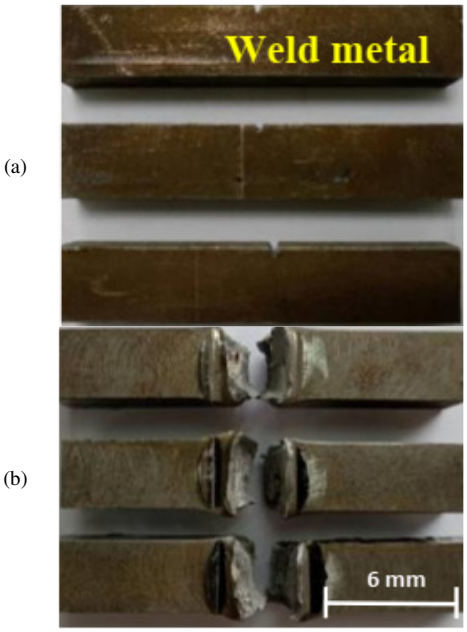

Fig. 15. Characteristics of specimen before and after impact testing at the weld metal: (a) before fracture, (b) after fracture.

In addition, the chemical composition and fracture characteristics of the specimens were examined (Figure 16(a)). The analysis revealed that manganese (Mn) exhibited the highest concentration, reaching 1.32 wt% (Figure 16(b)). At higher magnification, dimpled fracture patterns were observed (Figure 16(c)), which are indicative of shear failure and ductile fracture resulting from the applied shear forces.

The fracture characteristics of the specimens in the HAZ before and after Charpy testing are portrayed in Figure 18. In addition, the chemical composition and fracture morphology of the specimens were analyzed, as displayed in Figure 17(a). The results indicate that manganese (Mn) exhibited the highest concentration, reaching 1.72 wt% (Figure 17(b)). At higher magnification, the fracture surface reveals a cleavage-dominated morphology (Figure 17(c)), characteristic of brittle fracture behavior.

The amount of absorbed energy of all specimens that passed the impact test is shown in Figure 19 and Table IX. The average absorbed energy in the HAZ has the highest value of 256.57 J, while the average absorbed energy in the weld metal has the lowest value of 184.34 J. A larger and more uniform fracture area observed in the notch region of the HAZ indicates a higher capacity for impact energy absorption, whereas a narrower fracture area in the weld metal corresponds to a more abrupt and brittle fracture behavior [13].

TABLE IX. IMPACT TEST RESULTS ON THE SPECIMENS OBTAINED BY HYBRID GTAW AND SMAW WELDING

Location of Charpy V-notch	**Absorbed energy (J)**	
	Individual	Average
Weld metal	146.44	184.34
	211.56	
	195.03	
HAZ	305.56	256.57
	159.29	
	304.87	

D. Hardness Test

The results of the hardness test on the hybrid welding process, GTAW-SMAW, are portrayed in Figure 20. On the top line (red colour), the hardness trend across the 14 measurement points shows that the highest hardness value, 230 HV, was recorded at point 8 in the HAZ of the SMAW side, while the lowest hardness value, 173 HV, was observed at point 14 in the base metal region. At the test point positions 8-12 (HAZ), the hardness value was slightly higher than that of the weld metal. In contrast, the weld metal at test point positions 1–8 exhibited slightly higher hardness than the base metal at positions 12–14 [13, 14, 22].

The middle line (blue colour) shows that the highest hardness value of 210 HV was found at point 5 in the HAZ (SMAW), and the lowest hardness value of 141 HV was found at point 2 in the weld metal. From the test point positions 5-8 (HAZ), the hardness value was slightly higher than that of the test point positions 8-14 in the base metal, but the hardness value was slightly higher than that of the test point positions 1-5 in the weld metal [13, 14, 22].

The bottom line (green colour) shows that the highest hardness value, 231 HV, was observed at point 2 in the weld metal, while the lowest hardness value, 168 HV, occurred at point 11 in the base metal. At the test point positions 1-4 in the weld metal, the hardness value was slightly higher than in the HAZ (GTAW), but the test point positions 4-8 had a slightly higher hardness value than that of the test point positions 8-14 in the base metal [13, 14].

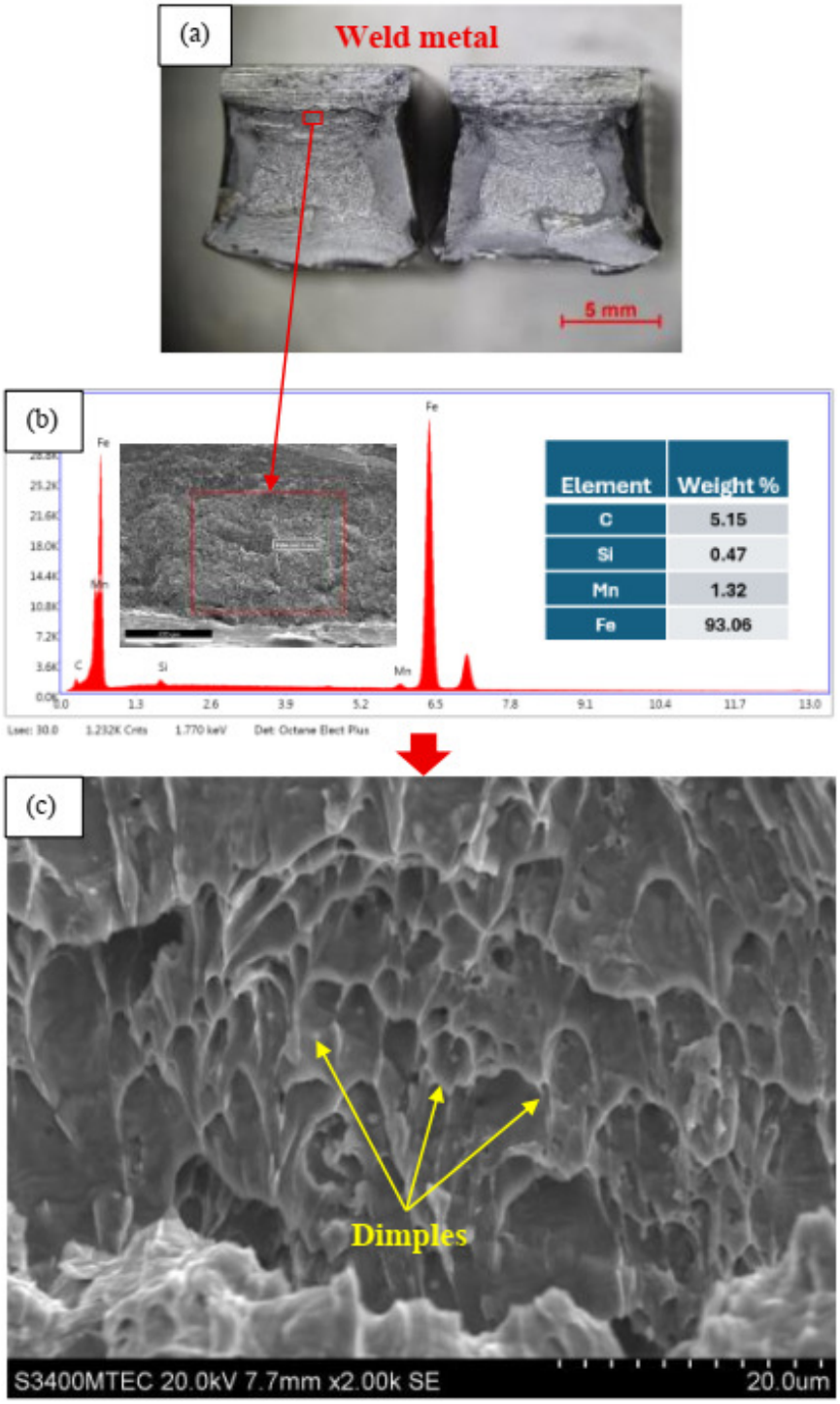

Fig. 16. SEM micrograph showing: (a) fracture characteristics of the impact test specimen at the weld metal, (b) EDS analysis results at the weld metal, (c) enlarged image of the crack area demonstrating the appearance of a hole in the crack (dimples) at a magnification of 2.00 kx. 20 µm.

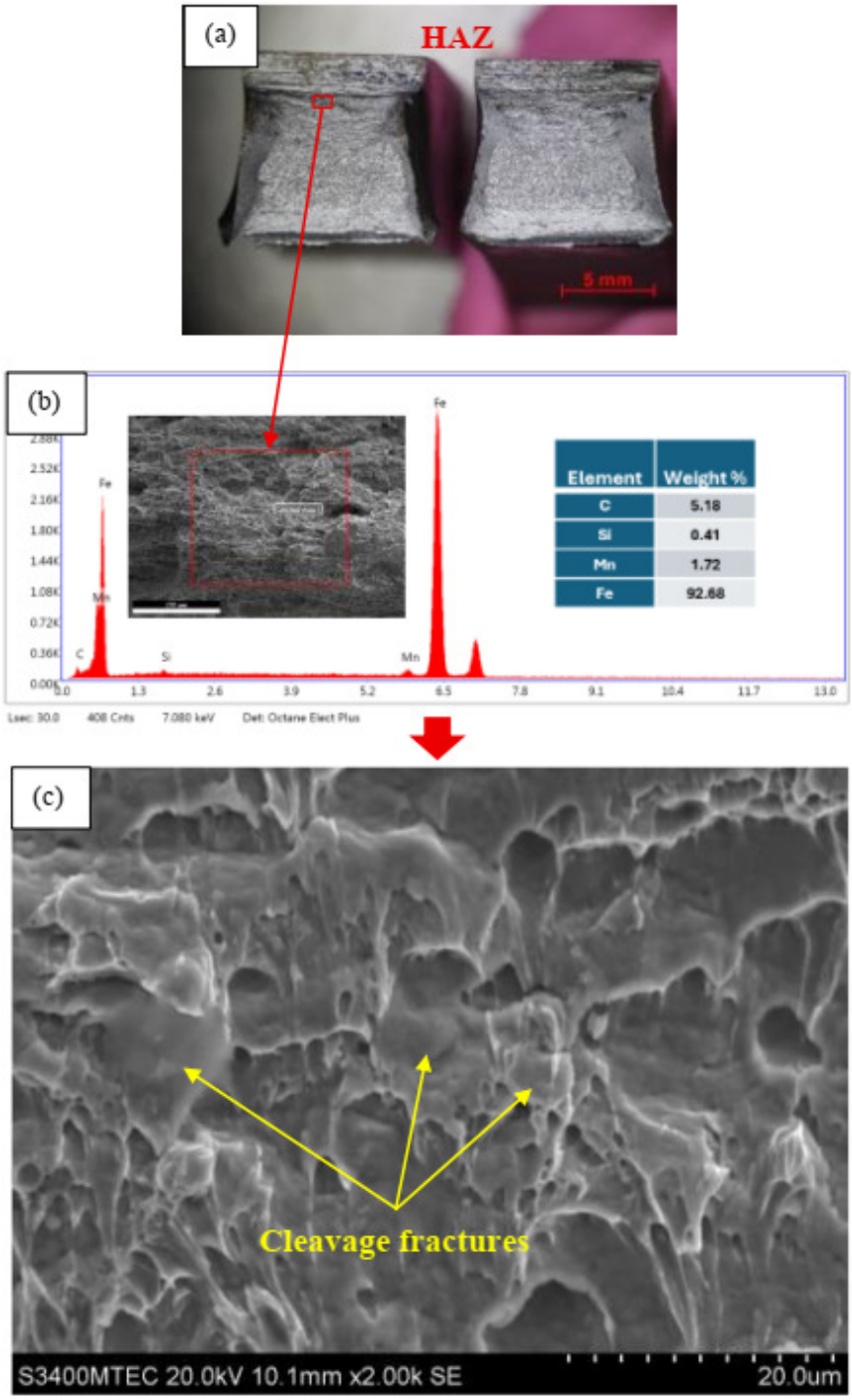

Fig. 17. SEM micrograph showing: (a) fracture characteristics of the impact test specimen at the HAZ, (b) EDS analysis results at the HAZ, (c) high magnification image with cleavage fracture at magnifications of 2.00 kx. 20 µm.

The results of the hardness test indicate that when the weld metal is subjected to heat during welding, its microstructure transforms into a solidified structure, leading to an increase in hardness. In the welding process, the HAZ, which is an area close to the welding metal, typically exhibits a lower hardness value than the weld metal but a higher hardness value than the base metal [13, 14].

E. Metallurgical and EDS Techniques

Figure 21 presents the microstructure of the base metal of EH36 steel. The microstructure consists of 82.23% ferrite (white) and 17.77% pearlite (black) [19].

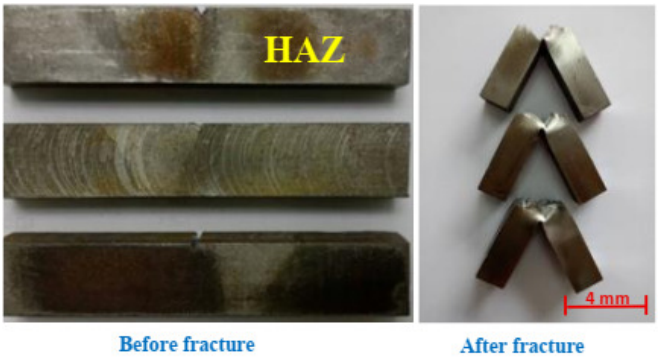

Fig. 18. Characteristics of the specimen before and after impact testing at the HAZ.

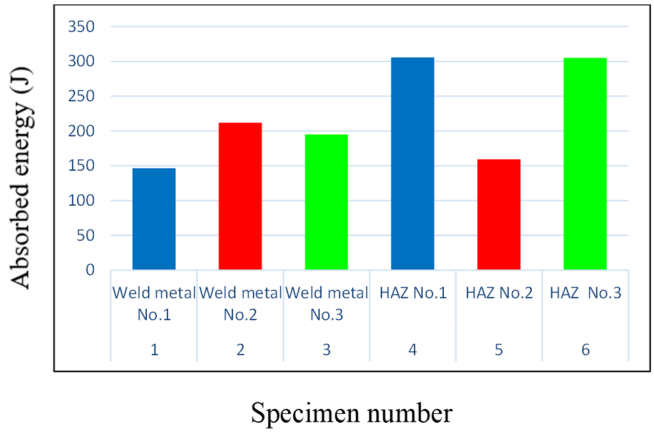

Fig. 19. Absorbed energy of the specimen after the Charpy impact test.

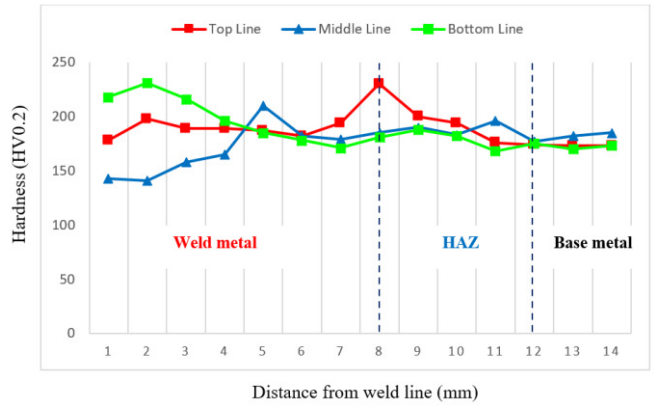

Fig. 20. Vickers' hardness test results for hybrid welding GTAW-SMAW.

Figure 22 presents the microstructure of the HAZ1 (SMAW). The microstructure consists of pearlite, ferrite, and bainite, where ferrite is the first phase formed, while pearlite and bainite are formed during the second phase [19].

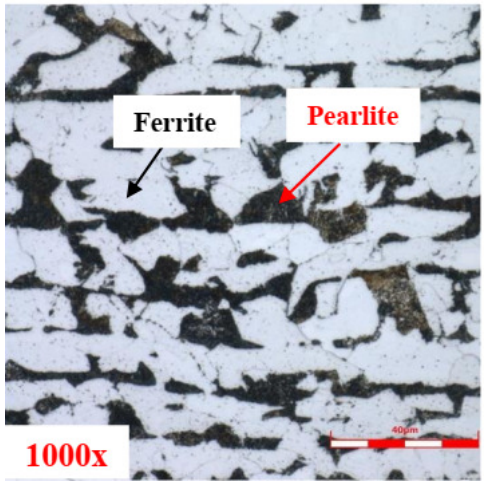

Fig. 21. Microstructure in the base metal of EH36 steel.

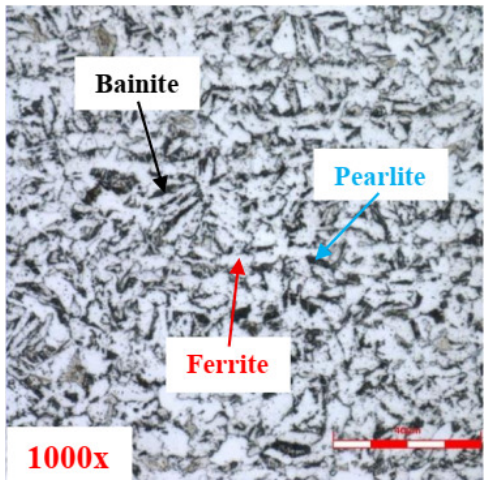

Fig. 22. Microstructure in the HAZ 1 (SMAW).

Figure 23 illustrates the microstructure of weld metal 1 (SMAW). The latter consists mostly of an acicular ferrite structure, with a polygonal ferrite (PF-I) structure inside the grain and a proeutectoid ferrite in the Widmanstatten ferrite structure [19]. In addition, its chemical composition was analyzed using the EDS technique. The results indicated that most detected elements originated from the filler metal. Manganese (Mn) showed the highest concentration, reaching 1.94 wt.%, which is close to and slightly exceeds the nominal composition specified for the AWS A5.18 ER 70S-6 filler metal. Accordingly, the measured Mn content confirms the use of ER70S-6 filler metal and plays a significant role in promoting the formation of acicular ferrite as the dominant microstructural phase in weld metal 1. The concentrations of the remaining elements are presented in Table X.

TABLE X. CHEMICAL COMPOSITION OF WELD METAL 1 (SMAW)

Element	**C**	**Si**	**Mn**	**P**	**S**	**V**	**Al**
%wt	0.16	0.18	1.94	0.016	0.005	0.012	0.048
Element	Cr	Cu	Mo	Nb	Ni	Ti	Fe
%wt	<0.005	<0.005	<0.003	0.012	0.009	0.055	Bal.

Figure 24 depicts the microstructure of weld metal 2 (GTAW) overlaid with SMAW. It consists of pearlite, ferrite, and bainite. The combined effect of these transformation mechanisms promotes the formation of a refined austenitic structure, which subsequently transforms into bainite under moderate cooling conditions [19]. In addition, its chemical composition was examined using the EDS technique. The chemical analysis revealed that most of the detected elements originated from the filler metal. Manganese (Mn) exhibited the highest concentration at 1.4 wt.%, followed by titanium (Ti) at 0.35 wt.% and chromium (Cr) at 0.30 wt.%. Consequently, the formation of bainite in weld metal 2 can be attributed to the relatively elevated Ti content (0.35 wt.%), together with Mn and Cr, which contribute to the increased weld metal hardenability. The composition of the remaining elements is summarized in Table XI.

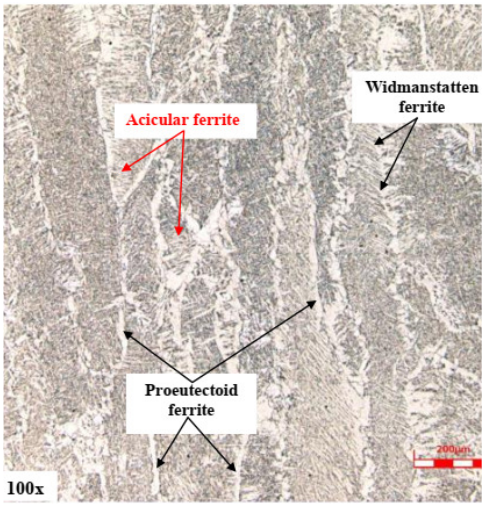

Fig. 23. Microstructure of weld metal 1 (SMAW).

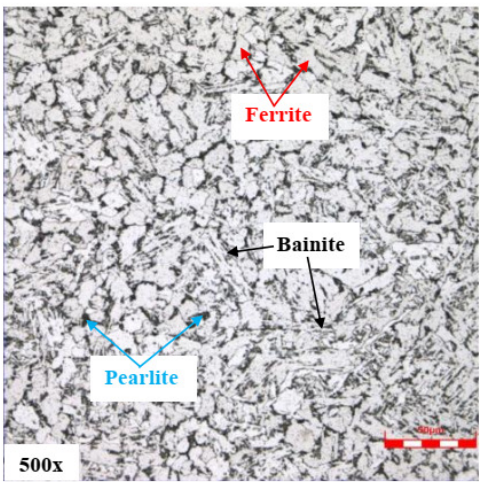

Fig. 24. Microstructure of weld metal 2 (GTAW).

Figure 25 shows the microstructure of the HAZ 2 (GTAW). It consists of 78.24% ferrite (white) and 21.76% pearlite (black) structures with fine-grain characteristics [19].

TABLE XI. CHEMICAL COMPOSITION OF WELD METAL 2 (GTAW)

Element	C	Si	Mn	P	V	Al	Cr
%wt	0.15	0.25	1.40	0.01	0.28	0.05	0.30
Element	Cu	Mo	Nb	Ni	Ti	Co	Fe
%wt	0.02	0.05	0.01	0.02	0.35	0.35	Bal.

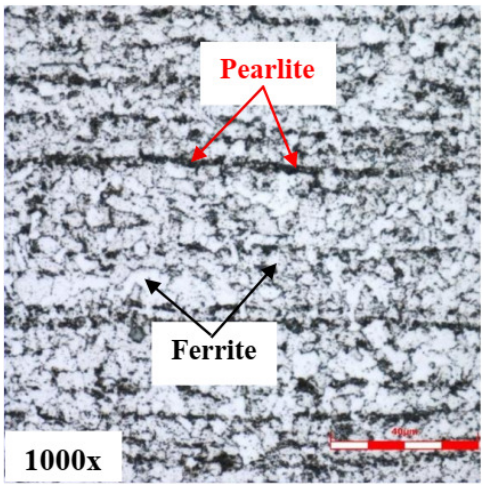

Fig. 25. Microstructure of HAZ 2 (GTAW).

IV. CONCLUSION

This research focused on the mechanical characteristics and metallurgical properties of EH36 steel butt joints produced by hybrid welding. The main drawn conclusions are:

- The microstructure of weld metal 1 Shielded Metal Arc Welding (SMAW) consists of acicular ferrite, polygonal ferrite, and proeutectoid ferrite. The Energy Dispersive Spectroscopy (EDS) technique revealed that several elements were present in the filler metal, with manganese being the most abundant element at 1.94%, followed by silicon at 1.18% in weld metal 1.
- The microstructure of weld metal 2 with Gas Tungsten Arc Welding (GTAW+SMAW) consists of pearlite, ferrite, and bainite. The EDS technique showed that many elements are components of the filler metal, with manganese being the highest element at 1.40%, followed by titanium at 0.35% and chromium at 0.30% in the weld metal 2.
- The tensile test results exhibited that the stress-strain curves of the welded specimens were close to each other due to the fracture of the specimens resulting from the tensile test. All fractures were found to occur in the Heat-Affected Zone (HAZ).
- Macrostructural examination of the three bend tests (side bend, face bend, and the root bend) demonstrated that all welded joints were free from cracks, fractures, tears, or other defects. This indicates that the welding process used for all samples is of high quality.
- The impact test results showed that the average absorbed energy in HAZ had the highest value of 256.57 J, while the average absorbed energy in the weld metal zone had the lowest value of 184.34 J. It can be concluded that the

average absorbed energy in the HAZ had better toughness than in the weld metal.

- The hardness test results revealed that the highest hardness value, 231 HV, was found in the weld metal, while the lowest value, 168 HV, was recorded in the base metal. The hardness of the weld metal was similar to that of the HAZ, but significantly higher than that of the base metal.

REFERENCES

[1] K. K. Um, S. H. Kim, K. B. Kang, Y. H. Park, and O. Kwon, "High Performance Steel Plates for Shipbuilding Applications," in *Eighteenth International Offshore and Polar Engineering Conference*, Vancouver, Canada, Jul. 2018, Art. no. ISOPE-I-08-317.

[2] F. Caiazzo *et al.*, "Laser Beam Welding of a Ti–6Al–4V Support Flange for Buy-to-Fly Reduction," *Metals*, vol. 7, no. 5, May 2017, Art. no. 183, https://doi.org/10.3390/met7050183.

[3] V. M. J. Varghese, M. R. Suresh, and D. S. Kumar, "Recent Developments in Modeling of Heat Transfer During TIG Welding—a Review," *The International Journal of Advanced Manufacturing Technology*, vol. 64, no. 5–8, pp. 749–754, Feb. 2013, https://doi.org/10.1007/s00170-012-4048-9.

[4] I. P. Wardani, V. A. Setyowati, S. Suheni, and I. P. Samudra, "The Effect of Welding Current on AISI 1045 Strength and Corrosion Rate," *Journal of Applied Sciences, Management and Engineering Technology*, vol. 1, no. 2, pp. 40–45, Nov. 2020, https://doi.org/10.31284/j.jasmet.2020.v1i2.1159.

[5] A. Jayant and M. Singh, "Use of Analytic Hierarchy Process (AHP) to Select Welding Process in High Pressure Vessel Manufacturing Environment," *International Journal of Applied Engineering Research*, vol. 10, no. 8, pp. 5869–5884, 2015.

[6] P. P. Thakur and A. N. Chapgaon, "Effect of GTAW-SMAW Hybrid Welding Process Parameters on Hardness of Weld," *International Journal of Engineering Research and Technology*, vol. 10, no. 1, pp. 782–786, 2017.

[7] J. C. F. Jorge *et al.*, "Influence of Welding Procedure and PWHT on HSLA Steel Weld Metals," *Journal of Materials Research and Technology*, vol. 8, no. 1, pp. 561–571, Jan. 2019, https://doi.org/10.1016/j.jmrt.2018.05.007.

[8] C. Li, G. Qin, Y. Tang, B. Zhang, S. Lin, and P. Geng, "Microstructures and Mechanical Properties of Stainless Steel Clad Plate Joint with Diverse Filler Metals," *Journal of Materials Research and Technology*, vol. 9, no. 2, pp. 2522–2534, Mar. 2020, https://doi.org/10.1016/j.jmrt.2019.12.083.

[9] I. R. Ibrahim, M. Khedr, T. S. Mahmoud, H. A. Abdel-Aleem, and A. Hamada, "Study on the Mechanical Performance of Dissimilar Butt Joints between Low Ni Medium-Mn and Ni-Cr Austenitic Stainless Steels Processed by Gas Tungsten Arc Welding," *Metals*, vol. 11, no. 9, Sept. 2021, Art. no. 1439, https://doi.org/10.3390/met11091439.

[10] D. Wang, P. Zhang, X. Peng, L. Yan, and G. Li, "Comparison of Microstructure and Mechanical Properties of High Strength and Toughness Ship Plate Steel," *Materials*, vol. 14, no. 19, Oct. 2021, Art. no. 5886, https://doi.org/10.3390/ma14195886.

[11] E. Korkmaz and C. Meran, "Mechanical Properties and Microstructure Characterization of GTAW of Micro-Alloyed Hot Rolled Ferritic XPF800 Steel," *Engineering Science and Technology, an International Journal*, vol. 24, no. 2, pp. 503–513, Apr. 2021, https://doi.org/10.1016/j.jestch.2020.04.006.

[12] S. Gook, A. Midik, M. Biegler, A. Gumenyuk, and M. Rethmeier, "Joining 30 mm Thick Shipbuilding Steel Plates EH36 Using a Process Combination of Hybrid Laser Arc Welding and Submerged Arc Welding," *Journal of Manufacturing and Materials Processing*, vol. 6, no. 4, Aug. 2022, Art. no. 84, https://doi.org/10.3390/jmmp6040084.

[13] S. Sirohi *et al.*, "Microstructure and Mechanical Properties of Combined GTAW and SMAW Dissimilar Welded Joints between Inconel 718 and 304L Austenitic Stainless Steel," *Metals*, vol. 13, no. 1, Dec. 2022, Art. no. 14, https://doi.org/10.3390/met13010014.

[14] S. Zhang, H. Wang, Y. Wang, and L. Cao, "Study on the Novel High Manganese Austenitic Steel Welded Joints by Arc Welding for Cryogenic Applications of LNG Tanks," *Materials*, vol. 16, no. 6, Mar. 2023, Art. no. 2381, https://doi.org/10.3390/ma16062381.

[15] D. G. Zisopol, M. Minescu, and D. V. Iacob, "A Study on the Influence of Aging of the Butt-Welded PE100 SDR11 on Shore A Hardness and Tensile Strength," *Engineering, Technology & Applied Science Research*, vol. 14, no. 1, pp. 12722–12727, Feb. 2024, https://doi.org/10.48084/etasr.6635.

[16] S. Nuchim, P. Bunyawanichakul, N. Angsuseranee, and V. Boonmag, "Residual Stress and Distortion Analysis for TMCP Steel Grade EH36 Butt Welding Parts in GTAW-SMAW Hybrid Welding Process Using Finite Element Method," *Engineering, Technology & Applied Science Research*, vol. 15, no. 1, pp. 20077–20084, Feb. 2025, https://doi.org/10.48084/etasr.8506.

[17] Norco Inc, *WELD 70S-6 AWS A5.18: ER70S-6*. Boise, ID, USA: Norco Inc, 2025.

[18] "Arc Welding Service," *Arc Welding Service Co.,Ltd.*, 2025. https://www.arcweldingservice.com/product/product_level/1/95/.

[19] T. M. Donizete Borba, W. Duarte Flores, L. De Oliveira Turani, and R. Cardoso Junior, "Assessment of the Weldability of EH36 TMCP Shipbuilding Steel Welded by High Heat Input Submerged Arc Welding," *Welding International*, vol. 31, no. 3, pp. 184–195, Mar. 2017, https://doi.org/10.1080/09507116.2016.1218619.

[20] "Metal Grades EH36 Grade Shipbuilding Steel.," *Metals USA*, 2025. https://www.metalsusa.com/eh36-grade-steel/.

[21] M. Staszuk and M. Nabialek, "Simularea Computerizata a Testului De Tractiune Statica Folosind Metoda Elementelor Finite," *Materiale Plastice*, vol. 54, no. 2, pp. 225–228, Jun. 2017, https://doi.org/10.37358/MP.17.2.4821.

[22] H. Zhang, C. Li, and Z. Zhu, "Influence of CDFW Process Parameters on Microstructure and Mechanical Properties of U75V Rail Steel Welded Joint," *Metals*, vol. 12, no. 5, Apr. 2022, Art. no. 711, https://doi.org/10.3390/met12050711.